Available online at www.sciencedirect.com
ScienceDirect
Journal of Power Sources 159 (2006) 1532–1542
JOURNAL OF POWER SOURCES
www.elsevier.com/locate/jpowsour

The capacitive characteristics of activated carbons—comparisons of the activation methods on the pore structure and effects of the pore structure and electrolyte on the capacitive performance

Feng-Chin Wu [a,*], Ru-Ling Tseng [b], Chi-Chang Hu [c], Chen-Ching Wang [c]

[a] *Department of Chemical Engineering, National United University, No.1, Lien Da, Kung-Ching Li, Miao-Li 360, Taiwan*
[b] *Department of Safety, Health and Environmental Engineering, National United University, Miao-Li 360, Taiwan*
[c] *Department of Chemical Engineering, National Chung Cheng University, Chia-Yi 621, Taiwan*

Received 24 June 2005; received in revised form 27 October 2005; accepted 14 December 2005
Available online 25 January 2006

Abstract

Fir wood-derived carbons activated with steam, KOH, and KOH + CO_2 were found to exhibit the high-power, low ESR, and highly reversible characteristics between −0.1 and 0.9 V in aqueous electrolytes, which were demonstrated to be promising electrode materials for supercapacitors. The pore structure of these activated carbons was systematically characterized by the *t*-plot method based on N_2 adsorption isotherms. Activated carbons prepared through the above three activation methods under different conditions (i.e., the gasification time of CO_2, KOH/char ratio, and activation time of steam) generally showed excellent capacitive performance in aqueous media, mainly attributed to the development of both micropores and mesopores (with the meso-pore volume ratio, V_{meso}/V_{pore}, ranging from 0.18 to 0.52). Scanning electron microscopic (SEM) photographs showed that the surface morphologies of honeycombed holes were found to depend on the activation methods. The average specific capacitance of the activated carbon with a combination of KOH etching and CO_2 gasification (with gasification time of 15 min) reached 197 F g^{-1} between −0.1 and 0.9 V in H_2SO_4. The capacitive characteristics of steam- and KOH-activated carbons in $NaNO_3$ and H_2SO_4 could be roughly estimated from the pore structure and BET surface area although the correlation may be only applicable for the fir wood-derived activated carbons.

Keywords: Activated carbon; Activation method; BET surface area; Pore structure; Surpercapacitor

1. Introduction

The physicochemical properties of activated carbons (ACs) have been found to strongly depend on the activation process and the nature of raw materials [1]. For instance, woods are ones of the most important materials for preparing ACs with particular porous characteristics, which are appropriate for the adsorption of solutes in liquid phase [2–4]. The BET surface areas and pore structures of wood-derived ACs, generally higher than those of ordinary ACs, were found to depend on the type of woods as well as the activation methods. For example, quercus agrifolia and eucalyptus woods activated with CO_2 were found to yield surface areas of 1201 and 1190 m^2 g^{-1} and pore volumes of 0.67 and 0.52 cm^3 g^{-1}, respectively [2,3]. In addition, rubber wood sawdust and wood flour activated with H_3PO_4 showed a BET surface area of 1780 m^2 g^{-1} and pore volume of 1.30 cm^3 g^{-1} [4]. Accordingly, an understanding on the influences of activation variables on the physicochemical properties of ACs is very important in developing the porous structure of various carbons in both physical and chemical activation processes [5]. The above viewpoints are especially important in the development of micro- and mesopores which can be strongly related to the adsorption capability/ability of ACs for various types of chemicals, gases or liquids. Actually, the high adsorption capacity of ACs is generally attributed to the properties of specific surface area, pore volume, and porosity. Hence, recent researches usually focus on the development of ACs with desired pore structures or the possibility of new application fields [6].

Activated carbons are important industrial materials for various applications [7–11]. Recently, the relationship between the porous structures and electrochemical behavior becomes important because carbons in various forms were used as elec-

* Corresponding author. Tel.: +886 37 381575; fax: +886 37 332397.
E-mail address: wfc@nuu.edu.tw (F.-C. Wu).

0378-7753/$ – see front matter © 2005 Elsevier B.V. All rights reserved.
doi:10.1016/j.jpowsour.2005.12.023

trode materials for surpercapacitors [7,12–14]. Since the cost of AC-based supercapacitors (i.e., electric double layer capacitors, EDLCs) is generally low [13], this type of energy storage devices are commercially attractive [15]. On the other hand, ACs manufactured under different conditions were found to have different pore structures and surface conditions that usually result in a loss in the electrochemically accessible surface area [12,15–17]. In addition, for the freely accessible surface areas, the specific capacitance ($\mu F\,cm^{-2}$) is not the same due to the presence of various functional groups [14,16]. Thus, many studies were carried out to modify the surface properties of ACs in order to optimize their capacitive performance (e.g., high power, low ESR, and high specific capacitance) [7,12–14,17,18].

For the high-power application purpose, the proportion of mesopores (i.e., 50 > pore diameter > 2 nm) within ACs is considered to be one of the key factors determining the capacitive performance of EDLCs since a complete array of the electric double layers can be easily established and the solvated ions can move freely within such pores. The above situations will cause a significant reduction in the equivalent series resistance (ESR) and a decrease in the electricity loss although a high proportion of mesopores will result in a loss of the specific surface area [14,16]. Moreover, the ESR is also attributable to the poor conductivity of ACs as well as the poor diffusion of solvated ions within micropores [12,15,17]. These characteristics depend mainly on the nature (e.g., graphite degree), the BET surface area, and the porous structure of carbons [12,15–18], which dictate the selection of activated carbon materials for supercapacitors [12,13,15].

The aim of this paper is to prepare various ACs from fir woods and to evaluate their applicability to supercapacitors. In addition, the physical properties such as BET surface area, pore size distribution, total pore volume, and micropore volume of carbons activated by means of three methods (i.e., steam activation, KOH etching, and KOH etching + CO_2 gasification) were systematically compared. Finally, the relationships between the physical properties and the capacitive behavior of these carbons were tried to establish.

2. Experimental details

2.1. Preparation of activated carbons with steam activation

Fir wood was dried at 110 °C for 24 h and then, placed in a sealed ceramic oven with a heating rate of 5 °C min^{-1} from room temperature to 450 °C. In the meantime, steam generated from deionized water (Millipore, Milli-Q) in a heating tube was poured into the oven for 1.5 h. After this heating step, steam was switched from the oven into the exhaust pipes. Under such oxygen-deficient conditions, the fir wood was thermally decomposed into hydrocarbon compounds and porous carbonaceous materials. This is the carbonization process.

In the subsequent activation process, the oven was further heated to 900 °C at 5 °C min^{-1} and kept at this temperature for 1, 3, 5 and 7 h. At the same time, the steam generated from deionized water at a flow rate of 3 cm^3 min^{-1} was poured into the oven for activation. After activation, the resulting dried carbons were cooled to room temperature and ground in a mill, washed with pure water, and finally dried at 130 °C. They were sieved in the size ranged from 0.12 to 0.2 mm. The steam-activated ACs prepared from fir wood for 1, 3, 5 and 7 h are denoted as FWST01, FWST03, FWST05 and FWST07, respectively.

2.2. Preparation of activated carbons with KOH activation

After the carbonization step as mentioned before, a weight ratio of 0.36 between char and fir wood was obtained. The chars of fir wood were removed, crushed, and sieved to a uniform size ranging from 0.83 to 1.65 mm. These powders were then mixed with water and KOH in a stainless steel beaker with the water:KOH:char weight ratios of 2:1:2, 2:1:1, 3:4:1 and 3:6:1, respectively. After drying at 130 °C for 24 h, the above mixtures were placed in a sealed ceramic oven, heated at a rate of 10 °C min^{-1} to 780 °C, and kept at this temperature for 1 h. In the meantime, N_2 gas was flowed into the oven at a rate of 3 dm^3 min^{-1}. The products were cooled to room temperature, washed with deionized water, and then, poured to a beaker containing 0.1 M HCl (250 cm^3) with stirring for 1 h. They were finally washed with hot water until pH of the washing solution reached 6–7 [19]. The carbons prepared from the fir wood with KOH activation at the KOH/char ratios of 0.5, 1, 4 and 6 are denoted as FWKC0500, FWKC1000, FWKC4000 and FWKC6000, respectively.

2.3. Preparation of activated carbons with KOH activation and CO_2 gasification

The same char powders handled in Section 2.2 were well mixed with water and KOH in a stainless steel beaker with a water:KOH:char weight ratio equal to 2:1:1. After drying at 130 °C for 24 h, the above mixtures were placed in a sealed ceramic oven, heated at a rate of 10 °C min^{-1} to 780 °C, and kept at this temperature for 1 h. In the meantime, N_2 gas was flowed into the oven at a rate of 3 dm^3 min^{-1} for various durations. When the KOH activation in N_2 reached the specified time, nitrogen gas was shut off and CO_2 gas was immediately introduced into the oven at a rate of 2 dm^3 min^{-1}. The total gas flow time for nitrogen and CO_2 into the oven at 780 °C was kept to be 60 min. Further treatments of these ACs were followed the same procedures handled in Section 2.2. The samples were classified according to the KOH/char ratio and the time duration of CO_2 gasification, which were denoted as FWKC1000, FWKC1015, FWKC1030 and FWKC1060, respectively (FW: fir wood; KC: KOH activation; 10: KOH/char ratio (=1.0); and the last two numbers represent the CO_2 gasification time in minutes).

2.4. Measurements of physical properties

The BET surface area of various carbons (S_p) was measured from the N_2 adsorption isotherms at 77 K with a sorptiometer (Porous Materials, BET-202A). Prior to this measurement, the samples were dried in an oven at 130 °C overnight and then, quickly placed into the sample tube. After that, the tube was heated to 230 °C and evacuated for 4 h until the pressure less than

1.33×10^{-4} mbar. The total pore volume (V_{pore}) was deduced from the adsorption data based on the Kelvin equation and the pore size distribution was derived from the BJH theory [20]. Although the BJH method is suitable for estimating the pore size distribution of mesoporous materials (≥2 nm), data of micropores presented in this work are relatively accurate, which are useful for comparison purposes. The micropore volume (V_{micro}) and external surface area (S_{ext}) were deduced by using the *t*-plot method [21]. The surface area corresponding to the micropores (S_{micro}) was obtained from the difference between S_p and S_{ext} [22].

2.5. Electrode preparation

Activated carbon powders were well mixed with 2 wt.% polyvinylidene difluoride (PVdF) binders for 30 min and *N*-methyl-2-pyrrolidone (NMP) was dropped into the above mixture and ground to form the coating slurry. This slurry was smeared onto the pretreated graphite substrates and dried in a vacuum oven at 50 °C overnight. In order to avoid any unexpected influences, the total amount of every AC paste on each electrode was kept approximately constant (ca. 2 mg cm^{-2}). The 10 mm × 10 mm × 3 mm graphite substrates before AC coatings were first abraded with ultrafine SiC paper, degreased with acetone and water, then etched in a 0.1 M HCl solution at room temperature (ca. 26 °C) for 10 min, and finally degreased with water in an ultrasonic bath. The exposed geometric area of these pretreated graphite supports is equal to 1 cm^2 while the other surface areas were insulated with PTFE (polytetrafluorene ethylene) coatings.

2.6. Capacitance measurements

The electrochemical measurements were performed through means of an electrochemical analyzer system, CHI 633A (CH Instruments). All experiments were carried out in a three- compartment cell. An Ag/AgCl electrode (Argenthal, 3 M KCl, 0.207 V versus SHE at 25 °C) was used as the reference and a piece of platinum gauze with an exposed area equal to 4 cm^2 was employed as the counter electrode. A Luggin capillary was used to minimize errors due to the *iR* drop in the electrolytes. The electrolytes used for the capacitive characterization were degassed with purified nitrogen gas for 25 min before measurements and this nitrogen was passed over the solutions during the measurements. The solution temperature was maintained at 25 °C by means of a water thermostat (Haake DC3 and K20).

3. Results and discussion

In order to gain an understanding on the influences of activation methods on the pore structure of ACs, the porous structure of various carbons has to be determined. Fig. 1 shows the typical N_2 adsorption/desorption isotherms for all ACs prepared in this work. In the case of steam-activated carbons, the adsorbed volume of N_2 is increased with increasing the activation time (t_A). The slope of the corresponding isotherms is also increased

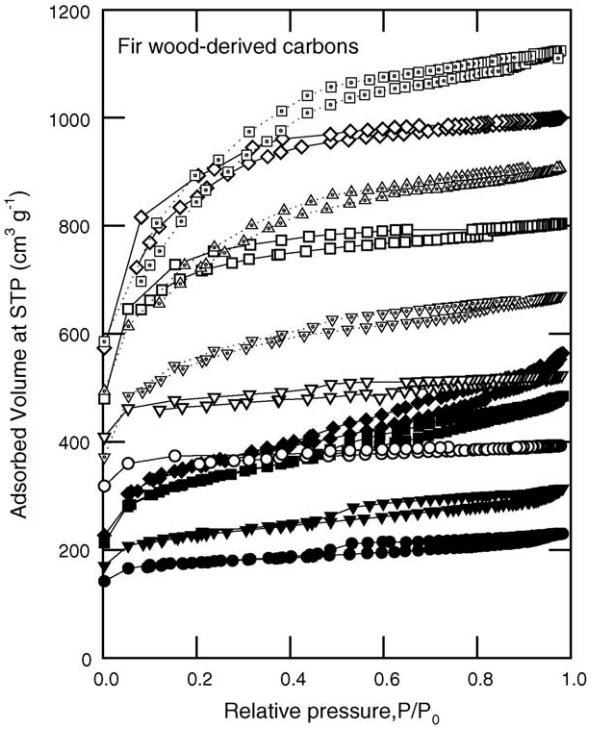

Fig. 1. Adsorption/desorption isotherms of N_2 at 77 K on activated carbons derived from fir wood prepared by steam, KOH, and KOH + CO_2 activation (the legends of all symbols are the same as those shown in Fig. 2).

with increasing the activation time. These results indicate that the size distribution of pores becomes wider with increasing the activation time (which has been discussed in Ref. [23]). For the KOH-activated carbons, with the exception of FWKC6000, the isotherms of N_2 adsorption/desorption at 77K become horizontal at $P/P_0 > 0.2$ (called Langmuir type). This reveals the formation of pores with a uniform size distribution (tubular pores). In addition, the adsorbed volume of N_2 is found to increase with increasing the KOH/char ratio. For the ACs activated with KOH and CO_2, the slope of isotherms is found to increase with increasing the CO_2 gasification time (i.e., t_G), indicative of the fact that the size distribution of pores is gradually widened. Moreover, the adsorbed volume is also increased with increasing t_G. Interestingly, the above results for the KOH + CO_2-activated carbons show the combined characteristics of the pore structure of the steam- and KOH-activated carbons. This implies that both KOH activation and CO_2 gasification may occur simultaneously when the char-KOH mixtures were heated in the oven flowed with CO_2 at 780 °C.

According to the definition from IUPAC, pores are classified into three groups according to the pore diameter: micropores (<2 nm), mesopores (2–50 nm), and macropores (>50 nm). In addition, over 95% of the total surface area usually comes from the micropores for common ACs [24]. Thus, the pore size distributions of all ACs examined in Fig. 1 are shown in Fig. 2 to gain an understanding on the developed structure of various ACs. For curves 1–4 (i.e., for all steam-activated carbons), the pores distributed within these ACs are mainly composed of two groups: micropores and mesopores with the

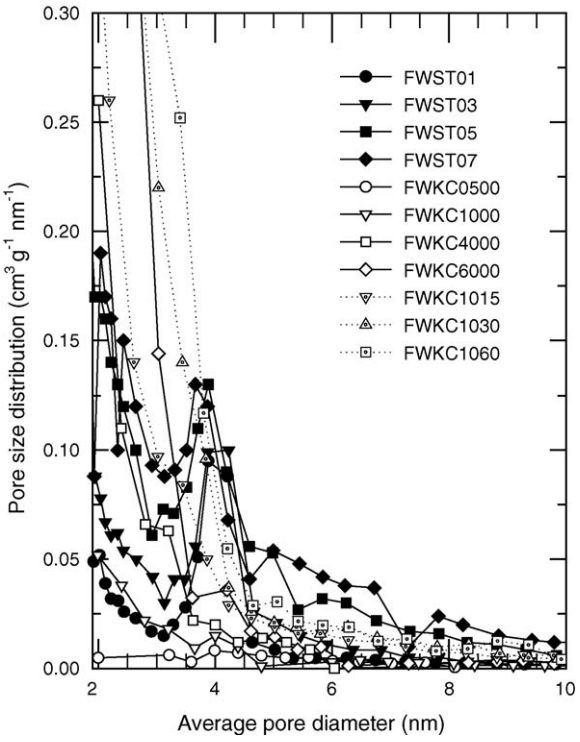

Fig. 2. The pore size distributions of activated carbons derived from fir wood prepared by steam, KOH, and KOH + CO_2 activation.

pore diameter centered at 4.0 nm. In addition, the amount of micropores is gradually increased and the mesopores with pore diameters from 2 to 4 nm are steadily developed with prolonging the activation time. Moreover, the mesopores with pore diameters ≥4.6 nm are also gradually developed with increasing t_A. Accordingly, micropores and mesopores within the wood-based carbons are simultaneously developed by the steam activation method. For curves 5–8 (i.e., for FWKC0500, FWKC1000, FWKC4000 and FWKC6000, respectively), with the exception of FWKC6000, most pores are smaller than 2 nm (belong to micropores). In addition, the pore size distribution becomes wider with increasing the KOH/char ratio. Actually, most pores within FWKC6000 are smaller than 4 nm, suggesting that the KOH/char ratio of 6.0 may be a critical value influencing the development of mesopores for the KOH activation process. From curves 9–11 (i.e., for FWKC1015, FWKC1030 and FWKC1060, respectively), on the other hand, a large proportion of mesopores was formed within these ACs (with the pore diameter ≤5 nm). Moreover, the pore size distribution is gradually widened with prolonging the gasification time.

The pore properties, including S_p, S_{ext}/S_p, V_{pore}, V_{meso}/V_{pore}, and D_p, of the ACs prepared from the above three activation methods are listed in Table 1. In the case of steam-activated carbons, prolonging t_A leads to an increase in the S_p, S_{ext}/S_p, V_{pore}, and V_{meso}/V_{pore}. When the activation time is prolonged from 1 to 7 h, S_p is increased from 528 to 1131 m^2 g^{-1}; V_{pore} is increased from 0.35 to 0.87 cm^3 g^{-1}; and V_{meso}/V_{pore} is increased from 0.33 to 0.52. These are typical properties of ACs with high ratios of mesopores, which have been discussed in our previous work [23]. In the case of KOH-activated ACs, increasing the KOH/char ratio from 0.5 to 6 renders an increase in S_p from 891 to 2794 m^2 g^{-1}, in V_{pore} from 0.61 to 1.54 cm^3, and in V_{meso}/V_{pore} from 0.18 to 0.24. Furthermore, an increase in the S_{ext}/S_p is also found with increasing the KOH/char ratio. Based on these results and the pore size distribution data, micropores are easily developed through the KOH activation, resulting in the high ratio of micropores within these KOH-activated carbons. For the KOH + CO_2-activated carbons, prolonging t_G also leads to an increase in S_p, S_{ext}/S_p, V_{pore}, and V_{meso}/V_{pore}, indicating the continuous development of pores in various diameters (from Fig. 2). As t_G is increased from 0 to 60 min, S_p is increased from 1371 to 2821 m^2 g^{-1}; V_{pore} is increased from 0.81 to 1.73 cm^3 g^{-1}; and V_{meso}/V_{pore} is increased from 0.20 to 0.38, indicative of the gradual transformation of micropores into mesopores.

The variation of D_p (average diameter of pores, $4V_{pore}/S_p$) values with the activation methods is interesting. The D_p values of steam- and KOH-activated carbons vary from 2.7 to 3.1 nm

Table 1
Physical properties of activated carbons derived from fir wood prepared by steam, KOH and KOH + CO_2 activation

Carbon	KOH/char ratio	T_A[a] (°C)	t_A[b] in H_2O	t_K[c] in N_2	t_G[d] in CO_2	S_p (m^2 g^{-1})	S_{ext}/S_p	V_{pore} (cm^3 g^{-1})	V_{meso}/V_{pore}	D_p (nm)	Reference
FWST01	–	900	1	–	–	528	0.14	0.35	0.33	2.7	[24]
FWST03	–	900	3	–	–	699	0.18	0.48	0.39	2.8	[24]
FWST05	–	900	5	–	–	1016	0.27	0.95	0.49	2.9	[24]
FWST07	–	900	7	–	–	1131	0.28	0.87	0.52	3.1	[24]
FWKC0500	0.5	780	–	60	–	891	0.08	0.61	0.18	2.7	
FWKC1000	1	780	–	60	–	1371	0.09	0.81	0.20	2.4	
FWKC4000	4	780	–	60	–	2179	0.10	1.24	0.22	2.3	
FWKC6000	6	780	–	60	–	2794	0.11	1.54	0.24	2.2	
FWKC1015	1	780	–	60	15	1718	0.14	1.03	0.28	2.4	
FWKC1030	1	780	–	60	30	2240	0.15	1.40	0.30	2.5	
FWKC1060	1	780	–	60	60	2821	0.20	1.73	0.38	2.5	

[a] Activation temperature.
[b] Steam activation time (h).
[c] KOH activation time (min).
[d] CO_2 gasification time (min).

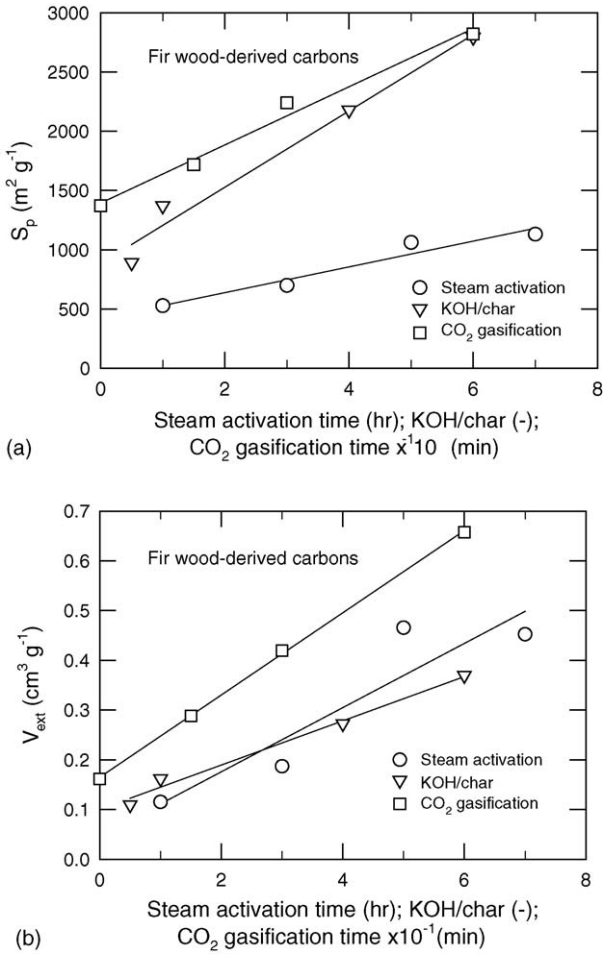

Fig. 3. (a) BET surface area, S_p; (b) exterior pore volume, V_{ext}, in activated carbons derived from fir wood prepared by steam, KOH, and KOH + CO_2 activation; CO_2 gasification time (□), KOH/char ratio (▽), and steam activation time (◯).

with prolonging t_A and vary from 2.7 to 2.2 nm with increasing the KOH/char ratio. On the other hand, the D_p values of ACs with a combination of KOH activation and CO_2 gasification are nearly constant (2.4–2.5 nm).

Fig. 3a and b show the dependence of S_p and V_{ext} of ACs on t_A, KOH/char ratio, and CO_2 gasification time (t_G), respectively. In Fig. 3a, the slope of S_p against t_A is much smaller than that of S_p against the KOH/char ratio. This is probably due to the more powerful etching rate of the chemical activation method in comparison with the physical activation one (see below). From a comparison of the dependence of S_p values on the CO_2 gasification time with the S_p value of FWKC1000, the S_p value is linearly increased with prolonging the CO_2 gasification time although the KOH/char ratio for these ACs is the same. This result may be due to the simultaneous formation of micro- and mesopores since KOH activation and CO_2 gasification may co-occur in the oven flowed with CO_2 at 780 °C.

Since the rate of pore development within ACs should depend on the feed amount of activation agent, the etching rate of different activation methods with the maximum feed amount of activation agents is compared here. Note that the etching rate of every activation agents can be simply expressed as follow:

$$r\,(\mathrm{m^2\,h^{-1}}) = \frac{\Delta S_P}{wt} \quad (1)$$

where w and t indicate the weight ratio of activation agent/char per hour, and the activation time, respectively. Since the specific surface area of chars is low in comparison with that of activated carbons used here, ΔS_p can be simply expressed as S_p.

For the steam activation, the flow rate of liquid water at room temperature is 3 $cm^3\,min^{-1}$, which corresponds to ca. 180 $g\,h^{-1}$ of water adding into the char. Since the total weight of chars during the steam activation is 48 g, the weight ratio of steam/char per hour is 3.75. For the KOH activation, the maximum weight ratio is 6.0. For the KOH + CO_2 activation, the flow rate of CO_2 at room temperature is 2 $dm^3\,min^{-1}$, corresponding to ca. 213 $g\,h^{-1}$ CO_2 (for 60 min gasification). Since the total weight of chars during the CO_2 + KOH activation is 16 g, the weight ratio of (CO_2+KOH)/char per hour is ca. 14.3. Based on Eq. (1), the developing rate of steam, KOH, and KOH + CO_2 activation is equal to 43.1, 465.7, and 197.3 $m^2\,h^{-1}$, respectively. Accordingly, the order of activation methods with respect to increasing the developing rate of surface area is: KOH > KOH + CO_2 > steam. Therefore, chemical activation methods, including the KOH activation and the combination of KOH activation and CO_2 gasification, are more powerful than the steam activation method in developing the pore structure of ACs.

In Fig. 3b, V_{ext} of the steam-activated carbons is rapidly increased with prolonging the time of steam activation while a relatively slow rate in developing V_{ext} is found for the KOH-activated carbons when the KOH/char ratio is gradually increased. These results suggest that the development of pores by the steam activation is bulkier than the method of KOH activation (i.e., relatively local etching). Hence, increasing the KOH/char ratio is mainly used to enhance V_{micro}. On the other hand, V_{ext} of the KOH + CO_2-activated carbons is increased rapidly with prolonging the time of CO_2 gasification. Based on the results and discussion for Fig. 3a and b, a combination of KOH activation and CO_2 gasification is a powerful method in developing the pores in various diameters for ACs.

3.1. Scanning electron microscopic (SEM) observations

Fig. 4a–g shows the SEM photographs of various carbons. The chars derived from fir wood (see Fig. 4a) show a perfect honeycomb structure with clear openings of pores and thick walls. After the steam activation for 7 h, the walls of honeycomb holes become thinner and partly fractured (see Fig. 4b, FWST07). Similar thinning in the wall of pores is also found for the KOH-activated carbons with the KOH/char ratios of 0.5 and 1.0 (see Fig. 4c and d for FWKC0500 and FWKC1000, respectively). Actually, a similar phenomenon was also found for corncob-derived activated carbons in our previous work [25], which has been attributed to the incomplete coverage of KOH on the surface of chars, resulting in the inefficient prevention of the wall surfaces from pyrolysis during the activation. On

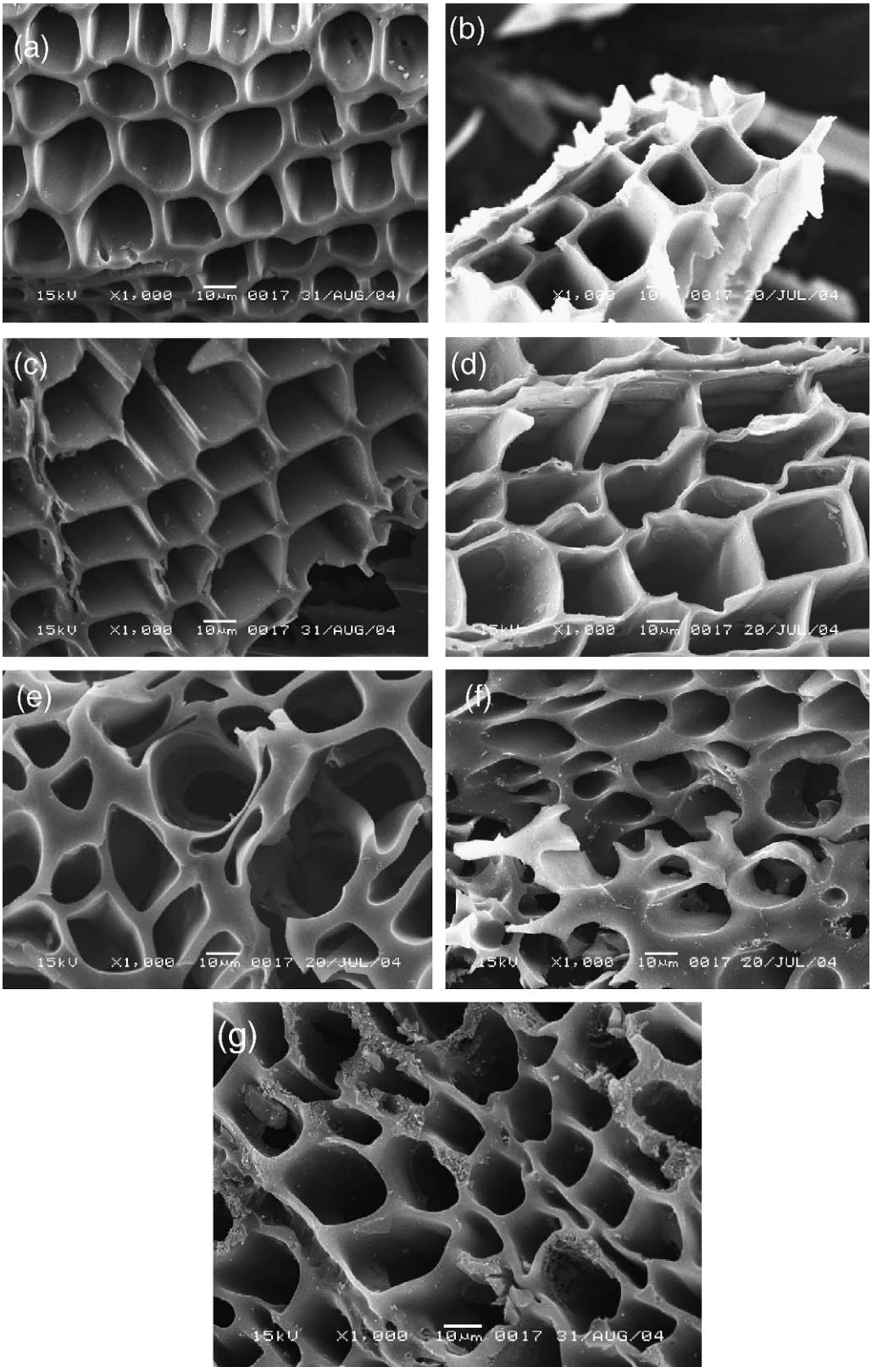

Fig. 4. SEM photographs (×1000) of (a) char; (b) FWST07; (c) FWKC0500; (d) FWKC1000; (e) FWKC4000; (f) FWKC6000; and (g) FWKC1030.

the other hand, the thick wall nature of honeycomb pores for FWKC4000 and FWKC6000 is maintained (see Fig. 4e and f) because the complete coverage of a KOH film on the surface of chars protects the attack of pyrolysis during the KOH activation [25]. For the KOH + CO_2-activated carbons, the openings of pores are clearly damaged and partly burnt, resulting in the thinning of walls (see Fig. 4g for FWKC1030). This is probably due to the violent attack of chars by CO_2 molecules since

a rising in the oven temperature about 20 °C during the initial 2 min when CO_2 was introduced. The above result is believed to be due to the incomplete coverage of KOH on the surface of chars, resulting in the inefficient prevention of the wall surfaces from pyrolysis during the activation [25] and the powerful ability of CO_2 gasification in developing the mesoporous structures of ACs.

3.2. Effects of electrolytes on the capacitive behavior of activated carbons derived from three activation methods

In our previous work [23], the specific capacitance of the steam-activated carbons was found to be proportional to their BET surface area and exhibited the application potential in supercapacitors. In addition, their capacitive performance was strongly influenced by the electrolytes employed. In order to gain an understanding on the effects of activation methods and electrolytes on the capacitive performance of ACs, all carbons prepared in this work were electrochemically characterized by means of cyclic voltammetry and chronopotentiometry in 1 M $NaNO_3$ and 0.5 M H_2SO_4. Typical results for the steam-, KOH-, and KOH + CO_2-activated carbons at 25 mV s^{-1} are shown in Fig. 5(a–f), respectively. An examination of Fig. 5, several features have to be mentioned. First, all *i–E* curves on the positive sweeps are generally symmetric to those on their corresponding negative sweeps. In addition, the voltammeric charges integrated from the positive sweeps are very close to their corresponding charges on the negative sweeps. These results indicate the excellent reversibility of the fir wood-derived carbons in aqueous media. Second, the voltammetric currents are gradually increased with prolonging the activation time of the steam-activated carbons or increasing the KOH/char ratio of KOH-activated carbons. In addition, the increase in voltammetric current is visible in the whole potential region, indicating that the capacitance mainly comes from the charge/discharge currents of the electric double layers. Accordingly, the increase in capacitive currents and specific capacitance are attributable to the increase in the BET surface area of ACs (see Table 1). Third, for the KOH + CO_2-activated carbons, the capacitive currents are sharply enhanced by the CO_2 gasification for only 15 min. However, the capacitance currents are obviously decreased with prolonging the CO_2 gasification time although the BET surface is directly proportional to the gasification time (see Fig. 3a). This abnormal phenomenon is never found in the literature, which will be further studied later in the temperature-programming desorption study. Fourth, the voltammetric currents rapidly reach their respective plateau values for all curves when the direction of potential sweeps is changed although the scan rate of CV is as fast as 25 mV s^{-1}. This indicates the relatively low equivalent series resistance (ESR) on most carbon-coated electrodes. A low ESR usually comes from a combination of a high electronic conductivity of electrode materials and a low ionic resistance of the electrolyte within the pores of ACs during the charge/discharge tests. Since the electronic conductivity of carbon materials are generally high meanwhile the presence of a large portion of mesopores within the steam- and KOH + CO_2-activated carbons should favor the movement and rearrangement of electrolytes within the pores, a low ESR for these carbon-coated electrodes is reasonable.

The effects of electrolytes on the electrochemical behavior of ACs with different structures can be clearly observed from a comparison of Fig. 5(a, c and e) and (b, d and f). Note that the capacitive currents obtained in the acidic solution are generally higher than that measured from the neutral electrolyte. This phenomenon is independent of the activation methods. The above difference in voltammetric currents is reasonably attributed to the better conductivity of the acidic electrolyte due to the proton hopping mechanism in aqueous media [26]. In addition, the excellent mobility of protons in the acidic solution should increase the electrochemically accessible surface areas of these highly porous carbons. On the other hand, the electrochemical reversibility of all carbons in $NaNO_3$ is better than that in the acidic electrolyte since the cyclic voltammograms obtained in the former electrolyte generally show a more rectangular-like shape. The above more capacitive-like and symmetric *i–E* responses indicate that fir wood-derived ACs exhibit excellent electrochemical characteristics for supercapacitors in 1 M $NaNO_3$. In addition, the fir wood-derived ACs is believed to exhibit a better power characteristic in the neutral electrolytes comparing with that measured in the acidic medium although the corresponding specific capacitance is certainly lower.

A comparison of Fig. 5b, d and f reveals the significance of activation methods on the capacitive performance of ACs. Note that the slope (i.e., *iR* drop) of the central, symmetric line on the CV curve can be roughly used to estimate the ESR of an electrode. The order of ACs with respect to increasing the ESR is: steam-activated carbons < KOH + CO_2-activated carbons < KOH-activated carbons although all ESR values are relatively low. Based on the fact that most pores within the KOH-activated carbons are microporous, the highest ESR of the KOH-activated carbons is attributable to the relatively poor ionic conductivity of electrolytes within the micropores of ACs. Moreover, the specific capacitance is not directly proportional to the BET surface area of ACs, especially for FWKC1060 with the highest BET surface area of 2821 m^2 g^{-1}. Also note that a pair of broad peaks between 0 and 0.5 V can be found on the CV curves of the steam- and KOH + CO_2-activated carbons, indicating the presence of a reversible redox couple in this potential region [16]. However, the redox peaks disappeared when CVs were measured in the neutral medium.

The effects of activation methods on the capacitive performance of ACs were further demonstrated by a comparison of their charge/discharge responses. Typical CP curves of FWST07, FWKC6000, FWKC1015, and FWKC1060 measured at various current densities in 1 M $NaNO_3$ are shown in Fig. 6a–d, respectively. In addition, the charge–discharge curves of FWKC1015 measured at the same current densities in 0.5 M H_2SO_4 are shown in Fig. 6e for a comparison purpose. In general, all charge and discharge curves measured from $NaNO_3$ show the mirror-like symmetric responses when the potentials are between −0.1 and 0.8 V. However, for the KOH- and KOH + CO_2-activated carbons, an irreversible oxidation is visible (especially clear at 3 mA cm^{-2}) at potentials positive to 0.8 V, while this phenomenon is not obvious for FWST07,

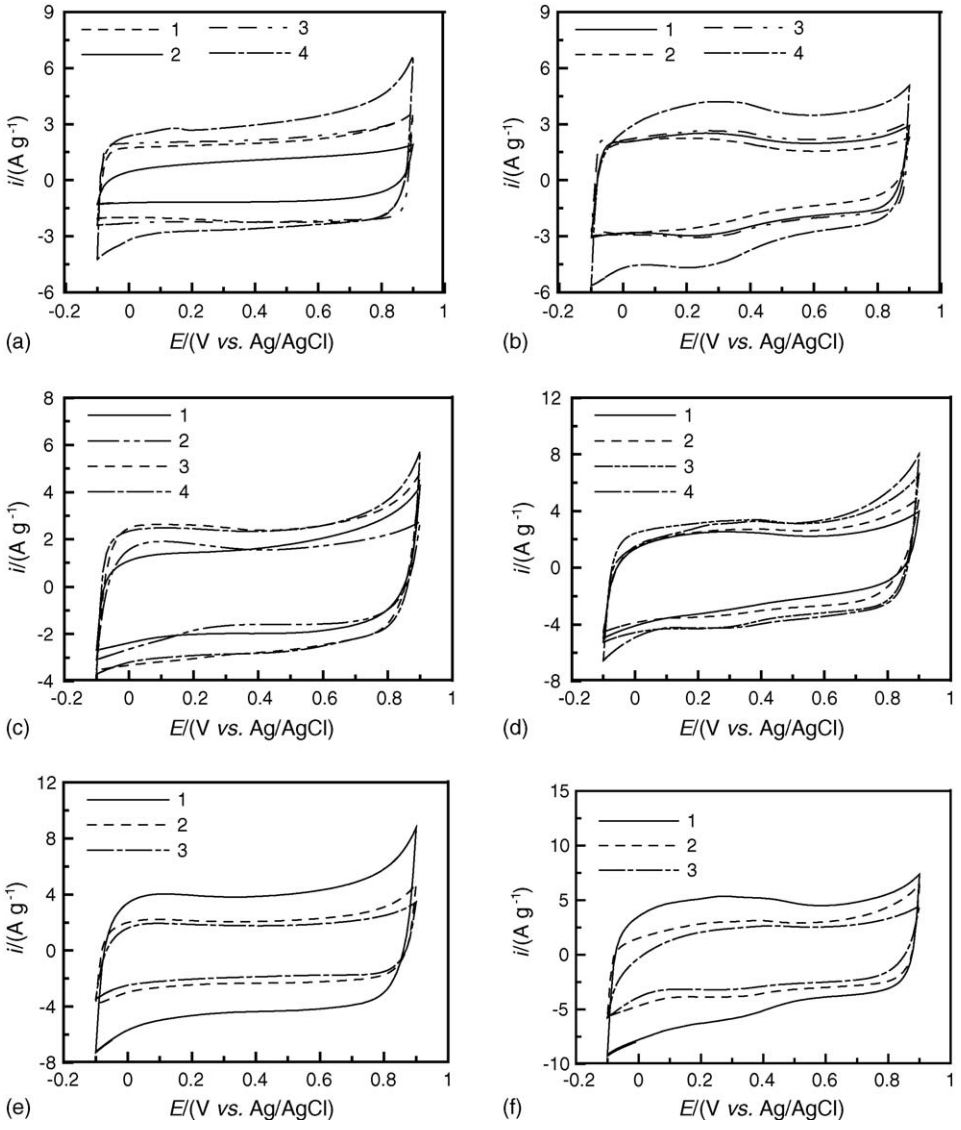

Fig. 5. Cyclic voltammograms of (a and b) steam-, (c and d) KOH-, and (e and f) KOH + CO_2-activated carbons measured in (a, c and e) 1.0 M $NaNO_3$ and (b, d and f) 0.5 M H_2SO_4. The steam activation time is equal to (1) 1, (2) 3, (3) 5, and (4) 7 h; the KOH/char ratio is equal to (1) 0.5, (2) 1, (3) 4, and (4) 6; and the CO_2 gasification time is equal to (1) 15 min, (2) 30 min, and (3) 60 min. All CV curves were measured at 25 mV s^{-1}.

indicative of the intrinsic nature of a steam-activated carbon. From Fig. 6e, the irreversible oxidation at potentials positive to 0.8 V on the charge curves is not clear while a gradual decrease in the slope (absolute value) is clearly found (especially clear at 3 mA cm^{-2}) on the discharge curves at potentials negative than ca. 0.4 V. This phenomenon suggests the presence of redox transitions on this KOH + CO_2-activated carbon, implying the significant contribution of pseudocapacitance coming from the redox transitions of surface functional groups (see below). The average specific capacitance of all carbon materials can be estimated on the basis of Eq. (2):

$$C_S = \frac{C}{w} = \frac{i}{|(dE/dt)|} \approx \frac{i}{(\Delta E/\Delta t)w} \quad (2)$$

where C_S, C, w, i, and (dE/dt) indicates the specific capacitance, average capacitance, weight of carbon, current density of charge/discharge, and the slope of these charge/discharge curves at a specific potential. In this work, the slopes of charge/discharge curves at a specific time are close to their mean values ($\Delta E/\Delta t$) of discharge curves.

The specific capacitances of various carbons obtained in 1 M $NaNO_3$ and 0.5 M H_2SO_4 are shown in Table 2. Note in Table 2 that a significant decrease in the specific capacitance with increasing the applied current density is found. This is probably due to the significant content of micropores within all activated carbons (see Fig. 2 and Table 1) although the proportion of mesopores within the steam- and KOH + CO_2-activated carbons is relatively high.

The ESR of all carbon-coated electrodes can be roughly estimated from the iR drop of CP curves when the applied current is altered. Moreover, the iR drops are more easily obtained under the highest current density of charge/discharge. In general, the iR drops obtained at the highest current density for all carbon materials are low (<82 mV). This indicates

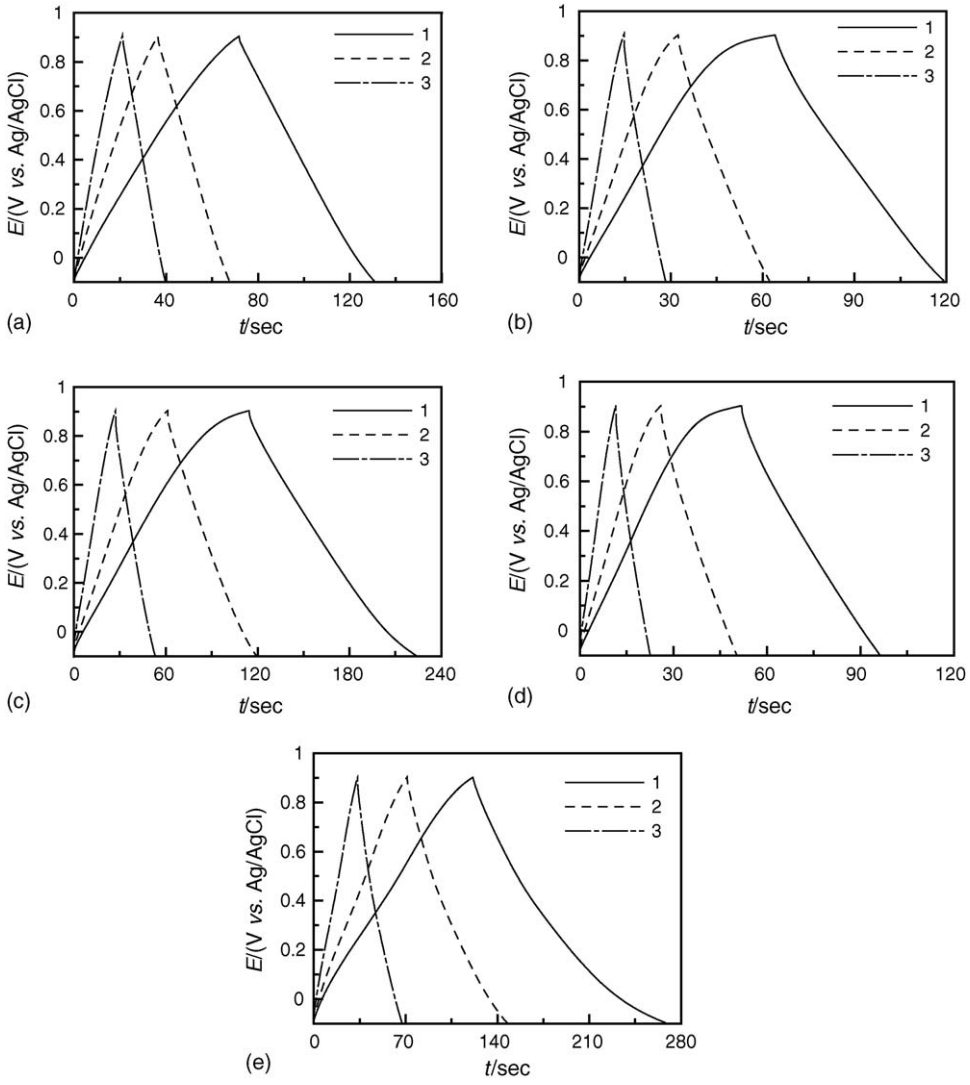

Fig. 6. Chronopotentiograms of (a) FWST07, (b) FWKC6000, (c) FWKC1015, and (d) FWKC1060 measured in 1 M $NaNO_3$ and (e) FWKC1015 measured in 0.5 M H_2SO_4 at (1) 3, (2) 5, and (3) 10 mA cm^{-2}.

Table 2
Specific capacitance of activated carbons derived from fir wood prepared by steam, KOH, and KOH + CO_2 activation; the applied current density is 3 mA cm^{-2}

Carbon	C_S (F g^{-1})	
	$NaNO_3$	H_2SO_4
FWST01	41	75
FWST03	82	89
FWST05	89	96
FWST07	114	142
FWKC0500	72	94
FWKC1000	68	106
FWKC4000	103	135
FWKC6000	104	138
FWKC1015	165	197
FWKC1030	92	127
FWKC1060	75	95

the low ESR values on these electrodes, which result from the good conductivity and mesoporous nature of all activated carbons prepared in this work. On the other hand, the order of carbons with respect to increasing the ESR is: FWST07 ≪ FWKC1060 ≈ FWKC1015 < FWKC6000. The lowest ESR of FWST07 also reveals the intrinsic nature of the steam-activated carbons for the application of supercapacitors in the aqueous solutions.

Based on the results shown in Tables 1 and 2, the dependence of the average specific capacitance measured in 1 M $NaNO_3$ and 0.5 M H_2SO_4 on the BET surface area of the steam-, KOH-, and KOH + CO_2-activated carbons can be clearly found in Fig. 7. Note that for both steam- and KOH-activated carbons, the specific capacitance (C_S) is directly proportional to their BET surface area. However, the slope for the steam-activated carbons (ca. 9.5 μF cm^{-2}) is much higher than that for the KOH-activated ACs (ca. 2.3 μF cm^{-2}). The former result indicates that the capacitance of both ACs should mainly come from the double-layer charge/discharge process that is directly proportional to

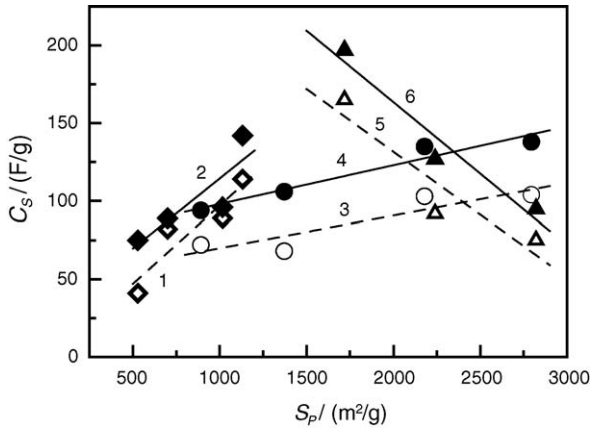

Fig. 7. The dependence of average specific capacitance measured in (1, 3 and 5) 1 M $NaNO_3$ and (2, 4 and 6) 0.5 M H_2SO_4 on the BET surface area of (1 and 2) steam-, (3 and 4) KOH-, and (5 and 6) KOH + CO_2-activated carbons.

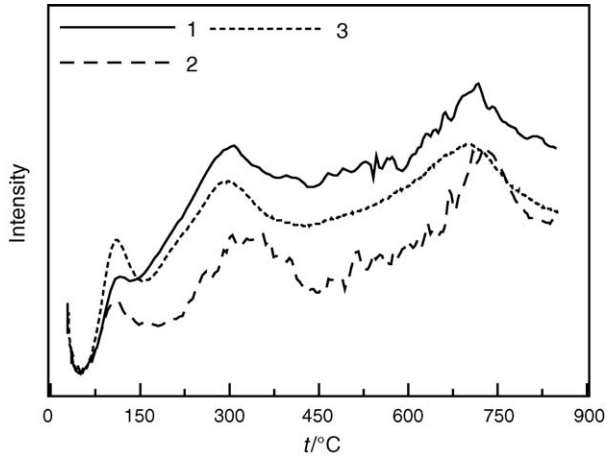

Fig. 8. Evolution profiles of CO_2 and CO by temperature-programming desorption for (1) FWKC1000, (2) FWKC1015, and (3) FWKC1060.

their electrochemically accessible surface area. The latter result suggests that in comparison with the KOH-activated carbons, a larger portion of the BET surface area for the steam-activated carbons is electrochemically accessible for electrolytes. This is probably due to that a large proportion of mesopores were developed in the steam-activated carbons (see Table 1). Actually, the dependence of C_S on S_p (or on V_{meso}/V_{pore}) of ACs should be not only affected by the activation methods but also by the starting materials [27]. Accordingly, the above correlation between C_S and S_p (or V_{meso}/V_{pore}) may be only applicable for the Fir wood-derived ACs. For the KOH + CO_2-activated carbons, on the other hand, although the proportion of mesopores within these activated carbons is increased with increasing the BET surface area, their specific capacitance are anomalously decreased with increasing the BET surface area, and the specific capacitance of FWKC1015 reaches the maximum (i.e., 165 and 197 F g^{-1} in $NaNO_3$ and H_2SO_4, respectively). In fact, Qu and Shi [14] found that the specific capacitances of certain ACs with BET surface areas of 2711 and 2130 m^2 g^{-1} are equal to 62.9 and 100 F g^{-1}, respectively. This phenomenon, interestingly, is similar to the case of our KOH + CO_2-activated carbons (i.e., a carbon with a higher specific capacitance has a lower BET surface area). However, based on the mechanism of double-layer charge/discharge, the specific capacitance of ACs should be directly proportional to their BET (specific) surface area [12,16,26]. If this is the case, the specific capacitance of FWKC1060 should be the maximum while an opposite phenomenon is clearly found for the KOH + CO_2-activated carbons. This anomalous result suggests that the specific capacitance of ACs with a combination of KOH activation and CO_2 gasification was not only contributed by the double-layer charge/discharge at the electrode–electrolyte interface but also by the redox transitions of surface functional groups (i.e., pseudo-capacitance). This statement is strongly supported by the extremely high C_S of FWKC1015.

Based on the above results and discussion, the distribution and density of the surface oxygen-containing functional groups within the KOH + CO_2-activated carbons need to be clarified, which was reported to significantly influence their performance in the energy storage and conversion systems [16,28]. Typical temperature-programming desorption (TPD) results of CO_2 and CO evolution for FWKC1000, FWKC1015, and FWKC1060 are shown in Fig. 8 since this technique is usually used to determine the distribution of oxygen-containing functional groups [27–29]. Based on Fig. 8, the surface of these chemically activated carbons is generally enriched with various oxygen-containing functional groups since the evolution of CO_2 (from anhydrides, lactones, and carboxyl groups [16,29,30]) and CO (attributable to quinone, hydroxyl, and carbonyl groups [16,29,30]) occurs predominately at temperatures below 550 and above 500 °C, respectively. From a comparison of these curves, several features have to be mentioned. First, FWKC1000 (i.e., the KOH-activated carbon) is enriched with all kinds of oxygen functional groups since the intensities of both CO_2 and CO evolution at temperatures above ca. 200 °C are higher than that of all KOH + CO_2-activated carbons. Accordingly, the CO_2 gasification can be used to remove the surface oxygen functional groups. Second, the "specific density" of surface functional groups (i.e., the intensities of CO and CO_2 evolution divided their corresponding BET surface areas) on FWKC1015 is higher than that of FWKC1060 since the loading of all ACs in the TPD study is the same. Both the above results suggest that CO_2 gasification is not only used to develop mesopores but also to remove the surface functional groups. Third, the intensities corresponding to CO evolution are generally higher than that of CO_2 desorption for FWKC1015 while the other two are enriched with all kinds of oxygen functional groups. This suggests that the surface of FWKC1015 is enriched with the electroactive groups (e.g., quinone, hydroxyl, and carbonyl groups). Based on the above TPD analyses and discussion, the density and distribution of oxygen functional groups on the surface of FWKC1015 should be very suitable, resulting in its highest specific capacitance. In addition, the possible mechanisms of redox transitions corresponding to these functional groups are simply expressed as follow:

$$O = Ph = O + 2H^+ + 2e \Leftrightarrow HO - Ph - OH \quad (3)$$

$$R = O + H^+ + e \Leftrightarrow R - OH \quad (4)$$

where Ph and R indicate the phenyl and aliphatic groups, respectively. Based on the above results and discussion, evolution of CO_2 and CO is visible for all chemically activated carbons while the density and distribution of surface oxygen functional groups are dependent on the activation method.

4. Conclusions

From the BET surface areas and the *t*-plot method, the steam- and KOH-activated carbons are mesoporous and microporous, respectively. The CO_2 gasification causes the transformation of KOH-activated carbons from microporous into the mesoporous structure and the partial removal of oxygen-containing functional groups. The highest BET surface area, $2821\,m^2\,g^{-1}$, is obtained from FWKC1060 (i.e., KOH activation and CO_2 gasification for 1 h). From SEM observations, the walls of honeycomb pores become thinner and partly fractured after the steam activation for 7 h. The coverage of KOH on the surface of chars causes the variation in the wall thickness of the honeycomb pores of the KOH-activated carbons. The activated carbons prepared from fir wood by the steam and $KOH + CO_2$ activation methods exhibit better capacitive performance (i.e., high-power, low ESR, and high reversible characteristics) between -0.1 and 0.9 V in aqueous electrolytes. The capacitive characteristics of all activated carbons obtained in $NaNO_3$ are much better than that measured in H_2SO_4 although the specific capacitance measured in the acidic solution is generally higher. The highest specific capacitance, $165\,F\,g^{-1}$ in $NaNO_3$ and $197\,F\,g^{-1}$ in H_2SO_4, of FWKC1015 demonstrated its application potential in supercapacitors. The capacitive characteristics of steam- and KOH-activated carbons in $NaNO_3$ and H_2SO_4 could be roughly estimated from their pore structure and BET surface area, while this correlation should be not only affected by the activation methods but also by the starting materials.

Acknowledgments

The financial support of this work, partially provided by the National Science Council of the Republic of China under contract no. NSC 92-2211-E-239-006 and NSC 93-2214-E-239-002, is gratefully acknowledged.

References

[1] W.T. Tsai, C.Y. Chang, S.Y. Wang, C.F. Chang, S.F. Chien, H.F. Sun, Resour., Conserv. Recycling 32 (2001) 43.
[2] R.S. Alejandro, A.E. Alfredo, L.T.S. Luis de, Carbon 39 (2001) 1367.
[3] N. Tancredi, T. Cordero, J. Rodriguez-Mirasol, J.J. Rodriguez, Fuel 75 (1996) 1701.
[4] H. Benaddi, T.Z. Bandosz, J. Jagiello, J.A. Schwarz, J.N. Rouzaud, Carbon 38 (2000) 669.
[5] D. Lozano-Castello, M.A. Lillo-Rodenas, D. Cazorla-Amoros, A. Linares-Solano, Carbon 39 (2001) 741.
[6] T. Kyotani, Carbon 38 (2000) 269.
[7] H. Shi, Electrochim. Acta 41 (1996) 1633.
[8] R.L. Tseng, F.C. Wu, R.S. Juang, Carbon 41 (2003) 487.
[9] W.T. Tsai, C.Y. Chang, S.L. Lee, Carbon 35 (1997) 1198.
[10] C.T. Hsieh, H. Teng, Carbon 38 (2000) 863.
[11] H. Fujimoto, A. Mabuchi, K. Tokumitsu, T. Kasuh, Carbon 38 (2000) 871.
[12] B.E. Conway, Electrochemical Supercapacitors, Kluwer-Plenum Publishing Co., New York, 1999.
[13] L. Bonnefoi, P. Simon, J.F. Fauvarque, C. Sarrazin, J.F. Sarrau, A. Dugast, J. Power Sources 80 (1999) 149.
[14] D. Qu, H. Shi, J. Power Sources 74 (1998) 99.
[15] A. Burke, J. Power Sources 91 (2000) 37.
[16] K. Kinoshita, Carbon, Electrochemical and Physicochemical Properties, John-Wiley & Sons, New York, 1988.
[17] C. Niu, E.K. Sichel, R. Hoch, D. Moy, H. Tennent, Appl. Phys. Lett. 70 (1997) 1480.
[18] J. Gamby, P.L. Taberna, P. Simon, J.F. Fauvarque, M. Chesneau, J. Power Sources 101 (2001) 109.
[19] Z. Hu, M.P. Srinivasan, Microp. Mesop. Mater. 27 (1999) 11.
[20] E.P. Barrett, L.G. Joyner, P.P. Halenda, J. Am. Chem. Soc. 73 (1951) 373.
[21] K.S.W. Sing, D.H. Everett, R.A.W. Haul, L. Moscou, R.A. Pierotti, J. Rouquerol, Pure Appl. Chem. 57 (1985) 603.
[22] R.S. Juang, R.L. Tseng, F.C. Wu, Adsorption 7 (2001) 65.
[23] F.C. Wu, R.L. Tseng, C.C. Hu, C.C. Wang, J. Power Sources 138 (2004) 351.
[24] M.S. El-Geundi, Adsorpt. Sci. Technol. 15 (1997) 777.
[25] R.-L. Tseng, S.-K. Tseng, J. Colloid Interface Science 287 (2005) 428.
[26] A. Bard, L.R. Faulkner, Electrochemical Methods, Fundamentals and Applications, John-Wiley & Sons, New York, 1980.
[27] F.-C. Wu, R.-L. Tseng, C.-C. Hu, C.-C. Wang, J. Power Sources 144 (2005) 302.
[28] C.-C. Wang, C.-C. Hu, Carbon 43 (2005) 1926.
[29] P.-Z. Cheng, H. Teng, Carbon 41 (2003) 2057.
[30] Y. Otake, R.G. Jenkins, Carbon 31 (1993) 109.